Analysis of Blood Flow Interacted with Leaflets in MHV in View of Fluid-Structure Interaction

Choeng Ryul Choi*†
Mechanical Engineering Department, Graduate School of Kyunghee University
Chang Nyung Kim
College of Mechanical & Industrial System Engineering, Kyunghee University

Interaction of blood flow and leaflet behavior in a bileaflet mechanical heart valve was investigated using computational analysis. Blood flows of a Newtonian fluid and a non-Newtonian fluid with Carreau model were modeled as pulsatile, laminar, and incompressible. A finite volume computational fluid dynamics code and a finite element structure dynamics code were used concurrently to solve the flow and structure equations, respectively, where the two equations were strongly coupled. Physiologic ventricular and aortic pressure waveforms were used as flow boundary conditions. Flow fields, leaflet behaviors, and shear stresses with time were obtained for Newtonian and non-Newtonian fluid cases. At the fully opened phase three jets through the leaflets were found and large vortices were present in the sinus area. At the very final stage of the closing phase, the angular velocity of the leaflet was enormously large. Large shear stress was found on leaflet tips and in the orifice region between two leaflets at the final stage of closing phase. This method using fluid-structure interaction turned out to be a useful tool to analyze the different designs of existing and future bileaflet valves.

Key Words : Mechanical Heart Valve (MHV), Hemodynamics, Fluid-Structure Interaction, Blood Flow, Pulsatile Flow, Shear Stress, Flutter

Nomenclature

$[C]$: Damping matrix
D_{ij} : Elasticity matrix
$\{F\}$: Force vector
$[IC]$: Influence coefficient
$[K]$: Stiffness matrix
$[M]$: Mass matrix
N_i : Shape function
$\{p\}_b$: Pressure at fluid-structure boundary
$\{q\}$: Displacement vector
$\{\dot{q}\}_b$: Velocity of structure at fluid-structure interface
Q : Flow rate
t : Time
u_i : Cartesian velocity component
U_j : Velocity component
x_i : Cartesian coordinate

Greek Letters

$\dot{\gamma}$: Shear rate
μ_s : Damping parameter
ρ_s : Density of the structure
θ : Leaflet angle

† First Author
* Corresponding Author,
E-mail : crchoi@cvs2.kyunghee.ac.kr
TEL : +82-31-201-2869; **FAX** : +82-31-202-8106
Mechanical Engineering Department, Graduate School of Kyunghee University, 1 Seochon, Kihung, Yongin, Kyunggi 449-701, Korea.(Manuscript **Received** June 23, 2000; **Revised** February 22, 2001)

1. Introduction

There are four different cardiac valves, that is, tricuspid valve, mitral valve, pulmonary valve and aortic valve. The function of these valves is to regulate the biologic blood flow and to avoid the regurgitation of blood. When these valves are malfunctioned, prosthetic heart valves are used for replacing cardiac valves.

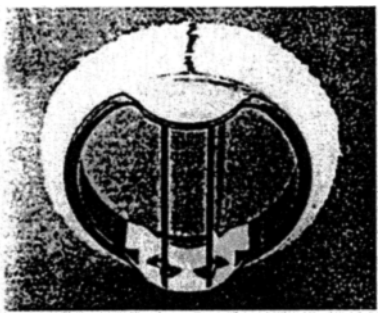

Fig. 1 Prototype of mechanical heart valve(St. Jude)

Bileaflet mechanical heart valves are the most commonly implanted prosthetic heart valves (Fig. 1). When the valve is fully open, high velocity jets through the gap between the leaflets can be readily detected both in vivo and in vitro (Chandran, 1985a; Woo et al., 1986; Hasenkam et al., 1988; Nygaard et al., 1994). The leaflets act as an obstruction to the blood flow through the valve and this, coupled with the high velocity jets through the leaflets, causes elevated shear stresses which may cause red blood cell damage or platelet activation. Together with high shear stress, increased coagulation due to blood stagnancy in contact with the artery walls may cause thrombosis and thromboembolism, which should be avoided for patients with prosthetic heart valve implant. An improvement of valve design requires a detailed understanding of these system properties and further substantial research. Analysis of the flow field around the valve may identify areas of flow disturbance and areas of stasis close to the valve and this information can then be used to improve current valve designs.

As in vivo experimental investigations are extremely difficult, most of researches have been performed through in vitro experimental studies and numerical simulations. Although many important aspects of hemodynamic aortic blood flow have been investigated in experimental studies (Sallam et al., 1976; Yoganathan et al, 1979; Skalak et al, 1982; Rossean et al., 1984; Tillman et al., 1984; Chandran et al., 1985b, Chandran et al., 1985c; Farahifar et al., 1985; Gross et al., 1988; Fatermi et al., 1989; Sikarskic et al., 1979), they lack spatial resolution, have problems analyzing transient phenomena or partially lack the detailed observation of theoretically interesting variables crucial for extended theoretical modeling because it is difficult to measure them. These partial drawbacks and limitations have suggested that numerical methods be of significant help in analyzing the dynamics of flowing blood.

Computational fluid dynamics (CFD) is an alternative tool that can be used to investigate the complex flow patterns within the valve and flow downstream of heart valves. Once a CFD model is defined and validated small changes can be made to one design parameter, such as the leaflet-opening angle, and the effect of this alteration on the flow field can be thoroughly investigated.

Many researchers have performed investigations on the flow field around the bileaflet mechanical heart valves using CFD (McQueen et al., 1985; Stevenson et al., 1985; King, 1994; King et al., 1994; Cerrolaza et al., 1997; Krafczyk et al., 1998; Gokhale et al., 1978; Imaeda et al., 1980). Previous studies have either ignored the effects of valve leaflet motion or approximated it using simplified assumptions, although the bileaflet mechanical heart valve cyclically performs open-and-close process due to the pulsatile flow caused by heartbeat. Therefore, they could not depict clearly the flow field and the leaflet motion for a complete cardiac cycle. To obtain reliable results, fluid-structure interaction between the fluid and the leaflets has to be included.

The present work investigates the blood flow through the bileaflet mechanical heart valve and the leaflet behavior associated with the blood flow for a Newtonian and non-Newtonian fluid cases using fluid-structure interaction analysis. A finite volume computational fluid dynamics code and a finite element structure dynamics code were used concurrently to solve the flow and structure equations, respectively, where the two equations were strongly coupled.

2. Numerical Method

The bileaflet mechanical heart valve cyclically performs open-and-close. To obtain the flow

field and the leaflet behavior for a cardiac cycle, the governing equations for fluid and structure are considered simultaneously.

2.1 Flow governing equations

The flow governing equations are the continuity equation and Navier-Stokes equation for an incompressible fluid. They can be written in a strong conservation form in the curvilinear coordinates as:

$$\frac{\partial}{\partial t}\left(\frac{\rho}{J}\right)+\frac{\partial}{\partial \xi^j}\left(\frac{\rho U_j}{J}\right)=0 \tag{1}$$

$$\frac{\partial}{\partial t}\left(\frac{\rho u_i}{J}\right)+\frac{\partial}{\partial \xi^j}\left(\frac{\rho U_j u_i}{J}\right)=-\frac{1}{J}\frac{\partial \xi^j}{\partial x_i}\frac{\partial p}{\partial \xi^j}+\frac{\partial}{\partial \xi^k}\left[\frac{\mu}{J}\frac{\partial \xi^k}{\partial x_j}\left(\frac{\partial \xi^l}{\partial x_j}\frac{\partial u_i}{\partial \xi^l}+\frac{\partial \xi^l}{\partial x_i}\frac{\partial u_j}{\partial \xi^l}-\frac{2}{3}\delta_{ij}\frac{\partial u_l}{\partial \xi^m}\frac{\partial \xi^m}{\partial x_l}\right)\right] \tag{2}$$

where u_i is the Cartesian velocity component, x_i is the Cartesian coordinate, U_j is the velocity component in the ξ^j direction (contravariant velocity component), and J is the coordinate transformation Jacobian. Futher,

$$x_1=x,\ x_2=y,\ x_3=z,\ \xi^1=\xi,\ \xi^2=\eta,\ \xi^3=\varsigma \tag{3}$$

$$U_j=\frac{\partial \xi^j}{\partial t}+\frac{\partial \xi^j}{\partial x_i}u_i=0 \tag{4}$$

where, $\frac{\partial \xi^j}{\partial t}$ represents the grid velocity, so that the above formulation is in an Eulerian-Lagrangian frame.

2.2 Structural Dynamics Governing Equation

Generally, the finite element formulation of the structural dynamics equation can be written as follows:

$$[M]\{\ddot{q}\}+[C]\{\dot{q}\}+[K]\{q\}=\{F\} \tag{5}$$

where $\{q\}$, $[M]$, $[C]$, $[K]$, and $\{F\}$ are the displacement vector, the mass matrix, the damping matrix, the stiffness matrix, and the force vector due to the fluid dynamic load and shear stresses, respectively:

$$[M]=\sum m^e{}_{ij}=\sum\int N_i\rho_s N_j dv \tag{6a}$$

$$[C]=\sum C^e{}_{ij}=\sum\int N_i\mu_s N_j dv \tag{6b}$$

$$[K]=\sum k^e{}_{ij}=\sum\int B_i D_{ji} B_i dv \tag{6c}$$

$$\{F\}=\sum\{f_i\}^2=\sum\int N_i p dv \tag{6d}$$

where N_i, ρ_s, μ_s, D_{ij} and are the shape function, the density of the structure, the damping parameter, and the elasticity matrix. B_i is related to N_i through a linear operator:

$$B_i=L_{ij}N_j \tag{7}$$

Newmark's scheme is applied to solve the above equation. For known values of q, $\dot{q}$, $\ddot{q}$ at (n-1)th time step, we have:

$$\{\dot{q}\}=\frac{2}{\Delta t}[[k]+\frac{4}{\Delta t^2}[M]+\frac{4}{\Delta t}[C]^{-1}\{F\}+\{E\} \tag{8}$$

where $\{E\}$ relates all the terms of q^{n-1}, $\dot{q}^{n-1}$, and $\ddot{q}^{n-1}$

2.3 Fluid-Structure Coupling

In the fluid Eq. (2), the structural effect comes into play only through the grid velocity term. This section will discuss the implicit coupling procedure. It is known that fluid velocity is always equal to the structure velocity and the contravariant velocity component in the Eulerian-Lagrangian formulation at solid-fluid boundary is zero:

$$U_j=\frac{\partial \xi^j}{\partial t}+\frac{\partial \xi^j}{\partial x_i}u_i=0 \tag{4}$$

If $\{\dot{q}\}_b$ is the velocity of structure at fluid-structure interface, then:

$$\{\dot{q}\}_b=-\frac{\partial \xi^j}{\partial t}=\frac{\partial \xi^j}{\partial x_i}u_i \tag{9}$$

On the other hand, Eq. (8) can be expressed in the following perturbation form:

$$\{\dot{q}\}'_b=[IC]\{p\}'_b \tag{10}$$

In light of Equation (9), we have

$$\frac{\partial \xi^j}{\partial x_i}u_i'=[IC]\{p\}'_b \tag{11}$$

where $[IC]$ and $\{p\}_b$ are the influence coefficient (Yang et al., 1994) and the pressure at fluid-structure boundary, respectively. When Eq. (11) is substituted into the pressure gradient term of pressure correction equation, the resulting equation depends only on flow variables.

Fluid velocities and pressures have been computed at each time step solving the Navier-Stokes

momentum and continuity equations. The fluid-structural dynamics model and fluid-structure interaction have been embedded in the iterative procedure. Fluid forces on the valve during each iteration are used to compute leaflet behavior. The leaflet surface velocity is imposed on the fluid in the altered flow domain during the next iteration. Fluid velocities and pressures are once again computed and the updated fluid forces on the leaflet are applied as structural boundary conditions. This process continues until both the flow variables and structural behavior converge to equilibrium values. The computational algorithm then proceeds to the next time step and the entire procedure is repeated. The rigorous scheme ensures fully coupled flow and structural solutions at each time step. A time accurate, backward Euler, upwind differencing SIMPLEC scheme is used in the flow solver.

3. Calculation Process

Two-dimensional, pulsatile blood flow interacted with leaflets motion has been analyzed numerically in a bileaflet mechanical heart valve (Fig. 1), which can be transplanted in place of aortic valve. Investigation has been carried out with the governing equations for blood flow and leaflet behavior, respectively, together with an auxiliary equation which couples the above equations. A commercial software package CFD-ACE+ ver. 6.0 and FEMSTRESS (a finite element structural analysis module) have been adopted. The numerical calculation with a 84×102 grid system and calculation time step of 0.0005s has taken about 30 hours to convergence with a PC of Pentium Ⅲ 600 and 256MB RAM. In fact, we performed with 60×86, 84×102 and 120×140 grid systems for grid sensitivity test, but the results were almost identical in both the cases with 84×102 and 120×140 grid systems. Since the blood can be regarded as a non-Newtonian fluids, comparison has been pursued for non-Newtonian and Newtonian blood flow ; for Newtonian blood flow, the density and the viscosity are and , respectively, and for non-Newtonian case, the density is and the viscosity

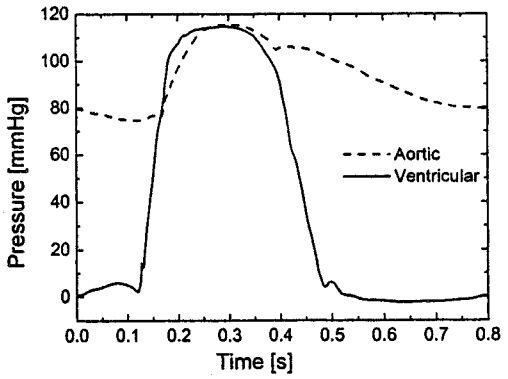

Fig. 2 Transient ventricular and aortic pressure waveforms at the boundaries

is calculated using Carreau model as follows.

$$\mu=\mu_\infty+(\mu_0-\mu_\infty)\cdot[1+(K\gamma)^a]^{\frac{n-1}{a}} \qquad (12)$$

where $\mu_0=1072\text{kg/m}\cdot\text{s}$, $\mu_\infty=0.006028\text{kg/m}\cdot\text{s}$, $n=0.3568\text{kg/m}\cdot\text{s}$, $K=2.6502\text{kg/m}\cdot\text{s}$, $a=2$, and γ is the shear rate.

St. Jude Medical Valve (SJMV), currently used bileaflet valve and made of pyrolytic carbon, is the model of the calculation, with internal diameter 22.5mm, leaflet thickness 0.65mm, closure angle 25°, wide open angle 85°. The diameter of aortic blood vessel is assumed to be 25.0mm. Geometry of the downstream region of MHV has adopted Sinus of Valsalva model suggested by Swanson et al.(1974).

ransient ventricular and aortic pressure waveforms, measured in vitro (Thubrikar et al, 1996a; Thubrikar et al., 1996b) with 75 beats per minute have been used as a pressure boundary condition for the numerical calculation (Fig. 2). At the vessel surface no slip condition is given for the blood flow and at the leaflet surface the velocity of the blood is the same as that of leaflet surface.

4. Results and Discussion

Transient variations in the leaflet opening angle and the leaflet angular velocity are shown in Fig. 3, where the time $t=0$ means the beginning of the opening phase of a leaflet associated with ventricular contraction (time $t=0$ in the

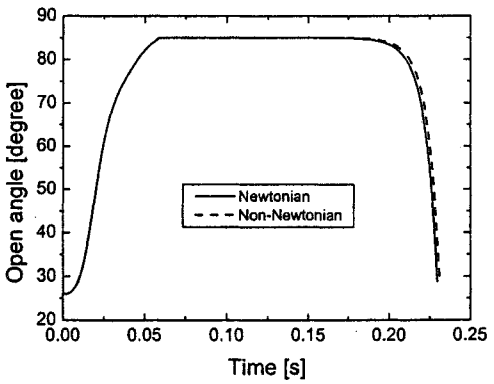

(a) Open angle

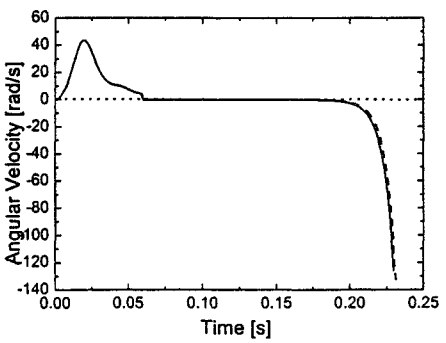

(b) Leaflet angular velocity

Fig. 3 Transient variation in the valve open angle and in the leaflet angular velocity

present calculation is equal to 0.164 s in Fig. 2). It is shown that the leaflet motion can be divided into five durations ; they are rapid opening, slow opening, fully opened, slow closing, and rapid closing. In the two cases of Newtonian and non-Newtonian fluids leaflets fluttering, the magnitude of which is an order of

10^{-4} degree, appears during fully opened phase. The fluttering is believed to be the result of numerical error caused by the succession of alternating use of computational fluid dynamics code and structural dynamics code in fluid-structure interaction, therefore it is not denoted in the figures.

For Newtonian fluid, the leaflet keeps fully opened during the period from t=0.0595 s to t= 0.1785 s with an angle of , and is closed at t=0. 2295s. For non-Newtonian fluid, the leaflet keeps fully opened during the period from t=0.0595s to

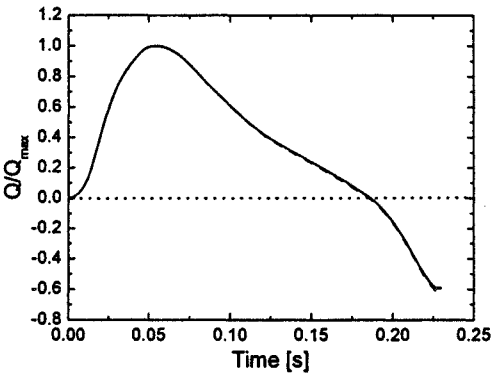

Fig. 4 Flow waveform normalized by the maximum flow rate

t=0.1815s, and is closed at t=0.231s. The variation of the leaflet behavior with fluid type is little. It can be noted that although the reverse pressure occurs at t=0.096s, closing phase starts at t=0. 1785s (Newtonian) and t=0.1815s (non-Newtonian), and that the angular velocity of leaflet at the final stage of closing phase is quite larger than in opening phase for both cases. The leaflet behaviors for Newtonian and non-Newtonian cases are generally similar.

Volumetric outflow rates in the ventricle, in conjunction with the pressure waves given in Fig. 2, have been calculated and been shown in Fig. 4. Reverse flow named closing regurgitation, starts to occur at t=0.1865 s (Newtonian) and t=0. 1860 s (non-Newtonian). It can be observed that the maximum flow rate occurs at t=0.0540 s (Newtonian) and t=0.0535 s (non-Newtonian), while the maximum pressure difference between the ventricle and the aorta occurs at t=0.0200 s. The amount of closing regurgitation is about 13% of the forward flow volume for a heartbeat. The flow rate shown in Fig. 4 may be used as boundary condition instead of pressure information for the analysis of blood flow around MHV.

Details of time-dependent blood flow for Newtonian fluid have been depicted in Fig. 5 for the whole domain; (a), (b), (c), and (d) correspond to the opening phase, the end of opening phase with the fully opened angle of , the end of fully opened phase meaning the starting point of

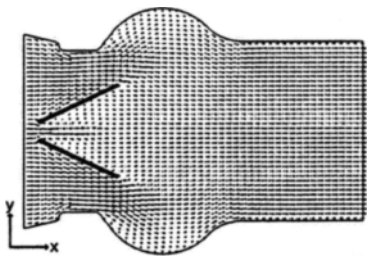

(a) θ=65°, t=0.0270s, MMV=1.101m/s

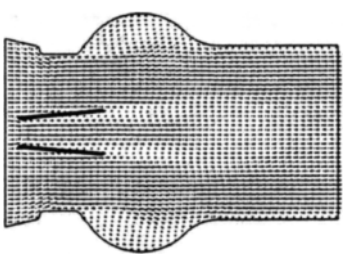

(b) θ=85°, t=0.0595s, MMV=1.268m/s

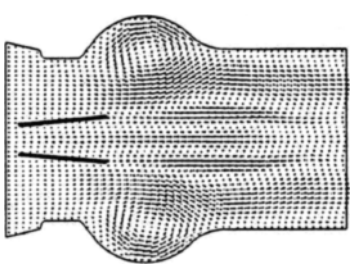

(c) θ=85°, t=0.1785s, MMV=0.326m/s

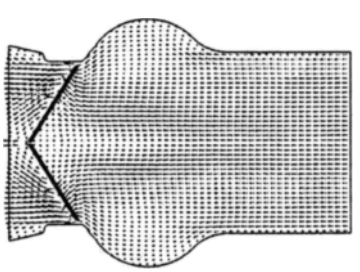

(d) θ=32°, t=0.2290s, MMV=1.667m/s

Fig. 5 Flow velocity vectors and leaflets behavior for Newtonian fluid(MMV: Magnitude of Maximum Velocity)

closing phase, and the final stage of closing phase, respectively. In the opening phase of Fig. 5(a) jet-like fast flow can be observed in the outer sides of two leaflets, however, almost uniform velocity can be seen downstream of the leaflets. In the fully opened phase (b) three jets are apparent between

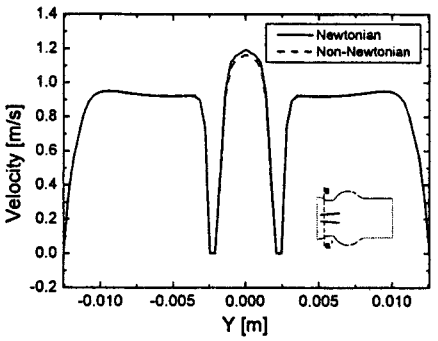

(a) Velocity

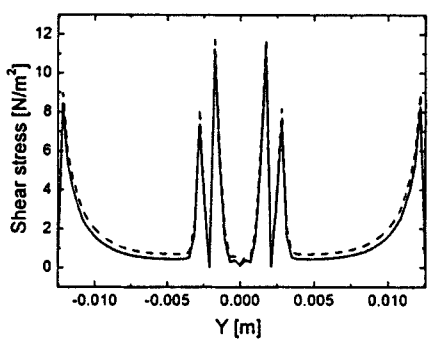

(b) Shear stress

Fig. 6 Velocity components and shear stresses in α -α'section(hinge) in the fully opened phase (θ=85°, t=0.0595s)

and outer sides of two leaflets. In this phase recirculation flow can be seen in the sinus, moving downstream with time. Reverse flow starts to occur in two narrow regions downstream of two leaflets (c) and propagates, as time goes, to the whole flow domain associated with the ventricular expansion (d). This reverse flow is considered to wash leaflet hinges, leaflet edges, and housing, reducing stasis and preventing formation of thrombus.

For fully opened phase velocities and shear stresses are shown in Fig. 6 and Fig. 7 for different sections, respectively, together with the velocities measured by King et al. (1996). In these figures, three jet-like flow is clearly seen and the maximum magnitude of jets is about 1. 2 m/s. The negative value of velocity in the sinus region appears also, meaning the existence of recirculation. In Fig. 7(a) the velocities show relatively poor agreement between the numerical

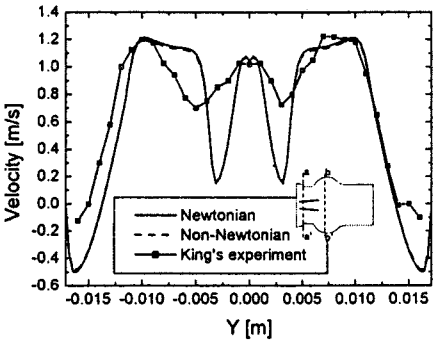

(a) Velocity

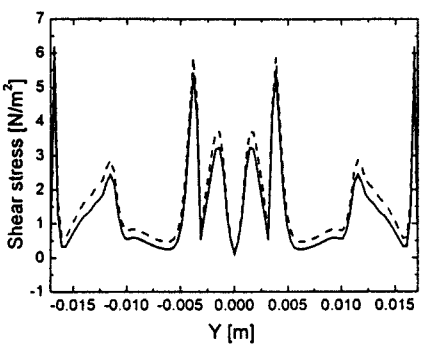

(b) Shear stress

Fig. 7 Velocity components and shear stresses in $b-b'$section(0.014m downstream of hinge) in the fully opened phase($\theta=85°$, $t=0.0595$s)

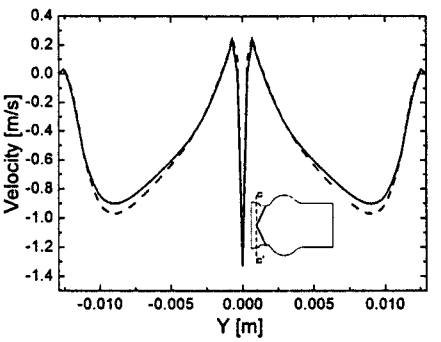

(a) Velocity

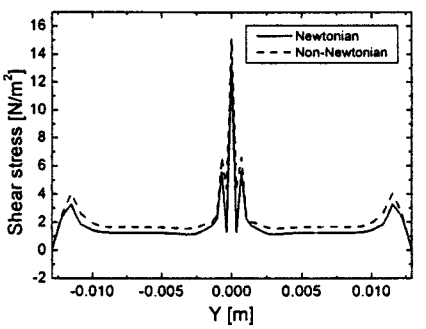

(b) Shear stress

Fig. 8 Velocity components and shear stresses in $c-c'$ section(0.0013m upstream of hinge) in the final stage of closing phase($\theta=32°$, $t=0.229$s)

and experimental results. The disagreement between both results is because King's experiment was performed with a Carbo Medics valve with a maximum opening angle and the data was obtained at peak systole. Due to the lack of experimental data performed with the identical boundary condition and valve in the literature, the exact comparison cannot be made for the present calculation. The present result and that of king's experimentation show qualitative agreement in the formation of three jets, though quantitative comparison may not be meaningful. Parallel experiments are in progress in our laboratories with the present calculation condition.

An important issue for valve hemodynamic analysis is shear stress level in the fluid in view of the platelet activation. From the present calculation, shear stress peaks are found around two leaflets and near housing. For the final stage of closing phase velocity components and shear stresses are shown in Fig. 8 and Fig. 9 for different sections, respectively. Here, jet-like reverse flow is found between two leaflets (Fig. 8), and between leaflet tip and the housing (Fig. 9). The peak values of each jet are -1. 4 m/s (between two leaflets as shown in Fig. 8) and -1. 6 m/s (between leaflet tip and housing as shown in Fig. 9). It can be noted that in the final stage of the closing phase the magnitude of the reverse flow velocity is quite larger than that of any other phase, related with the fast motion of leaflets at this very final part of the closing phase commented before. However, at the far downstream station, as depicted in Fig. 5, the velocity component along the blood vessel is rather smoothed out because of the convection/diffusion effects. Also, shear stress peaks are found between two leaflets in Fig. 8(b), and between leaflet tip

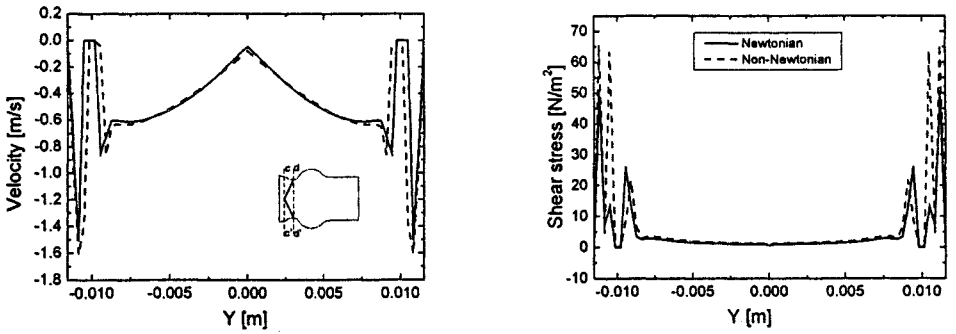

(a) Velocity (b) Shear stress

Fig. 9 Velocity components and shear stresses in $d-d'$ section(0.0042m downstream of hinge) in the final stage of closing phase($\theta=32°$, $t=0.229$s)

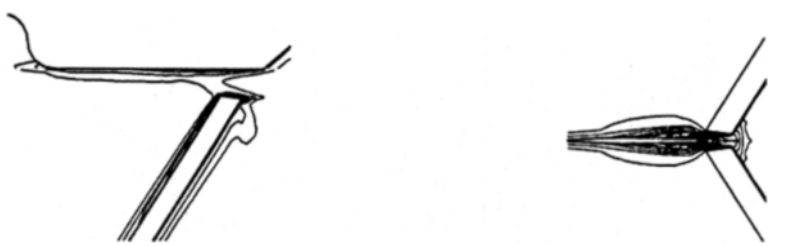

(a) Shear stress contour for Newtonian fluid($\theta=32°$, $t=0.229$s)

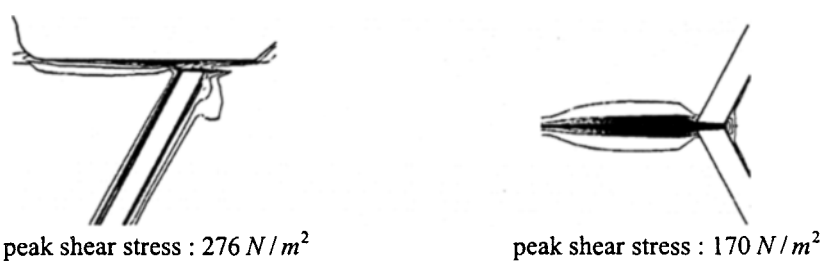

(b) Shear stress contour for non-Newtonian fluid($\theta=28°$, $t=0.231$s)

Fig. 10 Shear stress contours around the inner and outer tips of leaflets in the final stage of closing l phase

and the housing in Fig. 9(b). Considering shear stress in Figs. 6-9, shear stress for non-Newtonian fluid is generally higher than that for Newtonian case. Shear stress contours around the inner and outer tips of leaflets are shown in Fig. 10 at the very final stage of closing phase of the two different fluids. Maximum shear stress for non-Newtonian case is higher than that for Newtonian case. It can be noted that the shear stresses grow higher around leaflet outer tips than around leaflet inner tips.

5. Conclusions

The present work investigates the blood flow through the bileaflet mechanical heart valve and the leaflet behavior associated with the blood flow using fluid-structure interaction analysis. A finite volume computational fluid dynamics code and a finite element structure dynamics code have been used concurrently to solve the flow and structure equations, respectively, where the two

equations were strongly coupled. The present research aims to overcome the shortness of previous studies where the effect of leaflet motion has been ignored or approximated by simplified assumption, yielding unrealistic depiction of blood flow.

For Newtonian and non-Newtonian fluid, flow velocities, shear stresses, and leaflet behaviors have been obtained in the present calculation. For the two different cases, three jets are apparent through the mechanical heart valve with a recirculation in the sinus. For the final stage of closing phase, reverse flow velocity (closing regurgitation) is quite large between the two leaflets and between the leaflet and housing in association with high angular velocity of leaflet, causing high shear stress, being a source of concern in relation with platelet activation. Blood flows and leaflet motions are similar for Newtonian and non-Newtonian cases. However, shear stresses are a little higher for non-Newtonian case. The fluid-structure interaction turns out to be a reliable method for the design and/or analysis of mechanical heart valve prosthesis.

Acknowledgment

This study was supported by the KOREA RESEARCH FOUNDATION (Project number: KRF-99-042-F00127-F3300).

Reference

Cerrolaza, M., Herrera, M., Berrios, R. and Annicchiarico, W., 1997, "A Comparison of the Hydrodynamical Behaviour of Three Heart Aortic Prostheses by Numerical Methods," *J. Medicine Engineering and Technology(to appear).*

Chandran, J.B., 1985a, "Pulsatile Flow Past a St. Jude Medical Bileaflet Heart," *J. Thorac. Cardiovasc. Surg.*, 89, 743~749.

Chandran, K. B., Cabel, G. M, Khalighi. and Chen, C. J., 1985b, "Laser Anemometer Measurements of Pulsatile Flow Past Aortic Valve Prostheses," *J. Biomechanics*, 16(10), 865~873.

Chandran, K.M., Khalighi, B. and Chen, C.J., 1985c, "Experimental Study of Physiological Pulsatile Flow Past Valve Prosthese in a Model of Human Aorta-Ⅱ. Tiling Disc Valves and the Effect of Orientation," *J. Biomechanics*, 18(10), 773~778.

Farahifar, D., Cassot, F. and Bodard, H., 1985, "Velocity Profiles in the Weak of Two Prosthetic Heart Valves Using a New Cardiovascular Simulator," *J. Biomechanics*, 18(10), 789~802.

Fatermi, R.S. and Chandran, K.B., 1989, "An in Vitro Study of the St. Jude Medical and Edwards Duromedics Bileaflet Valve Using Laser Anemometry," *J. Biomech. Eng.*, 111, 298~302.

Gokhale, V.V., Tanner, R.J. and Bischoff, K.B., 1978, "FE solution for the Navier-Stokes equations for a 2D steady flow through a section of a canine aorta model," *J.Biomechanics*, 11, 241~249.

Gross, J.M., Shermer, C.D. and Hwang, N.H. C., 1988, "Vortex shedding in bileaflet heart valve prostheses," *Trans. Am. Soc. Artif. Intern. Organs*, 34, 845~840.

Hasenkam, J.M., Mygaard, H., Giersiepen, M., Reul, H. and Stodkilde-Jorgensen, H., 1988, "Turbulent Stress Measurements Downstream of Six Mechanical Aortic Valves in a Pulsatile flow Model," *J. Biomechanics*, 21. 631~645.

Imaeda, K. and Goodman, F., 1980, "Analysis of Non-linear Pulsatile Flow in Areries," *J. Biomechanics*, 13(8), 1007~1002.

King, M.J., Computational and experimental studies of flow through a bileaflet mechanical heart valve, Ph. D. Thesis. University of Leeds, UK, 1994.

King, M.J., Corden, J., David, T., and Fisher, J., 1996, "A Three-Dimensional, Time-Dependent Analysis of Flow Through a Bileaflet Mechanical Heart Valve : Comparison of Experimental and Numerical Results," *J. Biomechanics*, Vol. 29, No. 5, pp. 609~618.

King, M.J., David, T. and Fisher, 1994, "An Initial Parametric Study of Fluid Flow Through Bileaflet Mechanical Heart Valves Using Computational Fluid dynamics," *J. Eng. Med.*, 208, 63~71.

Krafczyk, M., Cerrolaza, M., Schulz, M. and Rank, E., 1998, "Analysis of 3d Transient Blood

Flow Passing Through an Artificial Aortic Valve by Lattice-Boltzmann Methods," *J. biomechanics*, Vol. 31, pp. 453~462.

McQueen, D. M. and Peskin, C., 1985, "Computer-Assisted Design of Butterfly Bileaflet Mechanical Heart valves for the Mitral Position," *J. Comput. Fluids*, 82, 289~297.

Nygaard, H., Paulsen, P. K., Hasenkan, J. M., Pedersen, E. M. and Rovsing, 1994, "Turbulent Stresses Down-Stream of Three Mechanical Aortic Valve Prostheses in Human Beings," *J. Thorac. Cardiovas. Surg.*, 107, 438~446.

Rossean, E.P. M., Van de Ven A.P . C., Van Steenhoven, A.A. and Seroo, J.M., 1984, "Design of a System for the Accelerated Loading of Heart Valve Prosthese," *J. Biomechanics*, 17(2), 145 ~153.

Sallam, L.A., Shaw, A. and Bain, W.H., 1976, "Experimental Evaluation of Mechanical haemolysis with Starr-Edwards, Kay-Shiley and BjorkShiley Valves," *Scandinavian J. Thoracic and Cardiovascular Surgery*, 10, 117~122.

Sikarskic, D.L., Stein, P. and Vable, M., 1979, "A mathematical for arotic valve vibration," *J. Biomechanics*, 17(11), 831~837.

Skalak, R., Finite elements in biofluid mechanics. FE Anaysis in Biomechanics, 1982.

Stevenson, D.M. and Yoganathan, A.P., 1985, "Numerical simulation of steady turbulent flow through trileaflet aortic heart valves-?. Computational scheme and methodology," *J. Biomechanics*, 18(12), 899~907.

Swanson, W.M. and Clark, R. E., 1974, "Dimensions and Geometric Relationships of the Human Aortic Valve as a Function of Pressure," *Cir. Res.*, Vol. 35, pp. 871~882.

Thubrikar, M.J., Selim, G, Robicsek, F. and Fowler, B, 1996a, "Effect of the sinus geometry on the dynamics of bioprosthetic heart valves(abstract)," *Ann. Biomed. Eng.*, 24, S3.

Thubrikar, M.J., Selim, G, Robicsek, F. and Fowler, B, 1996b, "Effect of the Sinus Geometry on the Dynamics of Bioprosthetic Heart Valves (abstract)," *Proceedings of the 18th Annual International Conference of the IEEE Engineering in Medicine and Biology Society Amsterdam, The Netherlands*, pg. 10 November.

Tillman, W., Reul, H., Herold, M., Bruss, K. H. and Van Gilse, J., 1984, "In vitro wall shear measurements at aortic valve prostheses," *J. Biomechanics*, 17(4), 263~279.

Woo, Y.R. and Yoganathan, A.P., 1986, "Pulsatile flow velocity and shear stress measurements on the St. Jude valve prosthesis," *Scand. J. Thorac. Cardiovasc. Surg.*, 20, 15~28.

Yang, H.Q. and Makhijani, V.B. 1994, "A strongly coupled pressure-based CFD agroithm for fluid-structure interaction," *Proceeding of 32nd Aerospace Sciences meeting and Exhibit*, Reno, NV, AIAA-94-0719.

Yoganathan, A.P., Coreoran, W. H. and Harrison, E. C., 1979, "In Vitro Velocity Measurements in the Vicinity of Aortic Prostheses," *J. Biomechanics 12*, 135~152.